Received: 5 February 2021 | Revised: 29 March 2021 | Accepted: 21 April 2021

DOI: 10.1111/ijag.16106

INTERNATIONAL JOURNAL OF Applied Glass SCIENCE

SPECIAL ISSUE ARTICLE

Alkali-free processing of advanced open-celled sinter-crystallized glass-ceramics

Hamada Elsayed[1,2] | **Patricia Rabelo Monich**[1] | **Gianpaolo Savio**[3] | **Malte Hartmann**[4] | **Aldo R. Boccaccini**[4] | **Dusan Galusek**[5,6] | **Jozef Kraxner**[5] | **Enrico Bernardo**[1]

[1]Department of Industrial Engineering, University of Padova, Padova, Italy

[2]Ceramics Department, National Research Centre, Cairo, Egypt

[3]Department of Civil, Environmental and Building Engineering, University of Padova, Padova, Italy

[4]Institute of Biomaterials, University of Erlangen-Nuremberg, Erlangen, Germany

[5]Joint Glass Centre of the IIC SAS, TnUAD, and FChFT STU, Trenčín, Slovakia

[6]FunGlass – Centre for Functional and Surface Functionalized Glass, Alexander Dubček University of Trenčín, Trenčín, Slovakia

Correspondence
Enrico Bernardo, Department of Industrial Engineering, University of Padova, Via Marzolo 9, Padova 35131, Italy.
Email: enrico.bernardo@unipd.it

Funding information
European Union's Horizon 2020 research and innovation programme, Grant/Award Number: 739566

Abstract

The cooling of a melt corresponding to the eutectic between wollastonite ($CaSiO_3$) and diopside ($CaMgSi_2O_6$) determines the synthesis of an interesting example of alkali-free bioactive glass, easily converted into glass-ceramics featuring two silicate phases, coupled also with åkermanite ($Ca_2MgSi_2O_7$), by sinter-crystallization of fine glass powders at 1000°C. The fabrication of scaffolds by digital light processing of glass powders suspended in a photo-curable, sacrificial binder, is a well-established technique; the present paper aims at disclosing novel approaches, concerning the topology of scaffolds, offering components with remarkable strength, especially in bending conditions. As an alternative, glass-ceramic foams were fabricated by the firing of porous precursors derived from the gelation of suspensions of glass powders in alkali-free basic aqueous solution.

KEYWORDS

additive manufacturing, alkali-free bioactive glasses, bioactive glass-ceramics, gel casting, scaffolds, sinter-crystallization

1 | INTRODUCTION

Bioactive glasses and glass-ceramics represent a fundamental group of bioceramics, having a distinctive combination of biocompatibility, bioactivity, and bioresorbability.[1-3] Among them, 45S5 bioactive glass has been widely studied for the development of scaffolds for bone tissue engineering.[3] 45S5 bioactive glass and other popular bioactive glass compositions, such as Biosilicate®,[4,5] feature a substantial content of Na_2O (>20 wt.%),[3] which may trigger a too high alkalinization of the medium upon degradation.[6]

A relatively recently established alternative class of biomaterials is represented by "alkali-free" bioactive glasses. Interesting examples are provided by silico-phosphate glasses

($CaO-MgO-SiO_2-P_2O_5-CaF_2$ system).[7-10] These glasses, depending on the formulation, may remain amorphous or crystallize into glass-ceramics featuring fluoro-apatite (a Ca-phosphate phase resembling the mineral component of bone, with F^- ions instead of OH^- ions) coupled with a Ca-Mg silicate phase, namely diopside ($CaMgSi_2O_6$). The coupling is quite classical, since silico-phosphate glass-ceramics crystallizing into wollastonite (Ca-silicate, $CaSiO_3$) and apatite, according to the investigations of Kokubo and coworkers,[3,11] were introduced as valid alternatives to 45S5 bioactive glass already in the early 1980s. However, it should be noted that the more recent investigations on alkali-free glass-ceramics have highlighted the specific role of Ca-Mg silicates, instead of simply wollastonite. Compared to wollastonite, Mg-containing systems show higher activation energy of Si ion release and thus a slower resorbability, exhibiting also better mechanical properties.[12]

The presence of a phosphate phase is not a necessary condition for a valuable bioceramic. Synthetic apatites, as an example, may exhibit lower bioactivity than that expected from their structural similarity with the mineral fraction of natural bone (only carbonate-doped apatite provides a closer match with the natural material).[13] "Phosphate-free" systems, featuring one or more silicate phases, are receiving a growing interest.[14] In particular, some systems may benefit from phases having different but complementary characteristics: highly soluble but mechanically weak wollastonite (W) may be coupled with less soluble but stronger diopside (D).[15] Interestingly, $CaSiO_3$ and $CaMgSi_2O_6$ form a eutectic (for a composition expressed by the molar ratio W:D = 52:48, e.g. by $CaO/MgO/SiO_2$ in the molar proportions of 33.2/16.0/50.8). A melt may be formed at relatively low temperature and then rapidly cooled into a glass.[16,17] The two silicate phases can be obtained by the viscous flow sintering of fine glass powders with concurrent crystallization ("sinter-crystallization").[18] In most cases, the two phenomena overlap when firing glass powder compacts at the glass crystallization temperature (T_{cryst}) or slightly above it.[19]

Sinter-crystallization has been widely shown as an opportunity for the processing of highly porous glass-ceramics. Viscous flow sintering enables a quite rapid consolidation of glass powders, whereas crystallization prevents the collapse of highly porous cellular structures. Such structures are defined by the same glass powders, distributed on sacrificial organic substrates (e.g., polyurethane sponges),[20] or embedded in porous polymer-glass composites.[21] Additive manufacturing (AM) technologies, involving the mixing of glass powders with sacrificial organic binders, are interesting for the preparation of cellular polymer-glass composite structures, later subjected to polymer burn-out and glass sinter-crystallization.[18]

The operating conditions for AM may interfere with the same sinter-crystallization process. More precisely, previous investigations showed that due to the limited packing of powders embedded in sacrificial photocurable resin, upon Digital Light Processing (DLP) experiments, sintering had to be performed at a much higher temperature than T_{cryst} (e.g., firing at 1100°C, with T_{cryst} = 920°C).[18] In other words, abundant voids between adjacent particles had to be recovered by enhancing the viscous flow. The present paper aims at illustrating a different strategy, based on the replacement of reticulated structures with triply periodic minimal surface (TPMS) architectures, enabling the achievement of scaffolds with remarkable strength-to-density even by firing at lower temperature (1000°C). In particular, we focused on gyroid structures, defined by the packing of helicoidal channels analogous to the one tested for titanium- and stainless steel-based nondegradable implants, manufactured by selective laser melting (SLM) and electron beam melting (EBM).[22,23] These structures were explored also for their potential for the manufacturing of graded materials, having a porous core sandwiched between denser surface layers.

The direct foaming of aqueous suspensions of fine glass powders ("gel casting approach"), in the field of porous glass-ceramic biomaterials, is certainly better established than any AM technology.[24] It specifically refers to the entrapment of air bubbles, through intensive mechanical stirring, followed by gelation, that is, a progressive increase in viscosity of the suspensions.[21,25,26] The gelation step implies the "freezing" of the cellular structure achieved by gas incorporation before the final consolidation by sintering. Fundamental differences in the approaches, besides the chemistry of the powders, depend on the additives promoting the gelation step. On the one hand, fully organic additives do not affect the chemical composition of the final product, but have rather complicated formulation (e.g., as reported by Wu et al., organic additives–dispersed in water–comprise acrylamide monomer coupled with N,N'-methylene bisacrylamide as cross-linker, ammonium persulfate solution as an activator and tetramethylethylene diamine as the catalyst).[21] On the other hand, the inorganic additives, such as Na and K hydroxides, determine an easy gelation, but also imply slight modifications of the chemical formulation, particularly negative in the perspective of really alkali-free biomaterials.[19] The present paper is dedicated also to the exploration of an alternative basic activator/gelation promoter, consisting of tetraethylammonium hydroxide ($[N(CH_2CH_3)_4]^+OH^-$, TEAOH): the simplicity of activation with NaOH or KOH is kept, but coupled with no modification of the adopted glass-ceramic formulation.

2 | MATERIALS AND METHODS

2.1 | Starting material

The reference glass (WDE glass), with $CaO/MgO/SiO_2$ in the molar proportions of 33.2/16.0/50.8,[18] was synthesized from

pure chemicals (silica, dolomite, calcium carbonate - all in powders <10 μm, Industrie Bitossi, Vinci, Italy), by melting at 1400°C, in a platinum crucible, for 1 h, with a heating rate of 10°C/min. The molten material was quickly solidified (quenched) by pouring the melt on a cold metal plate; coarse fragments were later reduced into fine powders, with a size below 38 μm, by dry ball milling and manual sieving.

2.2 | Fabrication of glass-ceramic scaffolds by means of additive manufacturing

STL (Standard Triangulation Language) models were prepared employing Rhinoceros® 6 program package (Robert McNeel & Associates, Seattle, WA, USA), according to the approach described by Savio et al.[27] These models described bars with dimensions 50 mm × 8 mm × 6 mm, and 75 vol% nominal porosity, in the form of uniform and gradient gyroids, illustrated by Figure 1A and B, respectively. In the gradient gyroid structure, the average porosity of 75 vol% was determined by the overlapping of layers with a porosity varying from 65% (top) and 85% (core), according to the profile shown in Figure 1C.

The developed STL models were implemented in a commercial DLP (digital light processing) printer (3DLPrinter-HD 2.0 machine, Robot Factory s.r.l., Mirano, Italy), to produce glass-resin composite scaffolds, in analogy with previous experiences.[18] Fine glass powders were suspended in a commercially available photocurable acrylic polymer (FunToDo Standard Blend, Lumi Industries S.r.l., Montebelluna Italy), already comprising a suitable photo-initiator and photo-absorber, for a solid load of 60 wt.%. The printer operated in the visible light range–between 400 and 500 nm -, with a layer thickness of 100 μm (exposition lasting 4 s for each layer). Samples were printed "horizontally," that is, they were determined by slicing along the largest surfaces (50 mm × 8 mm). After cleaning in an ultrasonic bath with isopropanol for 3 min, the samples were subjected to a secondary curing step, in a UV curing chamber (operating wavelength 365 nm, Robot Factory S.R.L., Mirano, Italy), for 15 min. Finally, the samples underwent a preliminary heat treatment in the air (1°C/min heating rate) at 550°C aimed at the burn-out of the photo-cured binder. Finally, the samples were sintered in air at 1000°C (5°C/min heating rate) for 1 h, followed by natural cooling.

2.3 | Fabrication of glass-ceramic foams by means of "basic" activation

"Green" glass foam samples were prepared by frothing an aqueous suspension of fine glass powders, for a solid loading of 60 wt.%, activated by addition of tetraethyl-ammonium hydroxide ($[N(CH_2CH_3)_4]^+OH^-$, TEAOH, reagent grade, Sigma-Aldrich, Gillingham, UK) in a concentration of 1 mol/L. Glass slurries were firstly kept under low-speed mechanical stirring (500 rpm) for 3 h to induce partial dissolution and gelation. Second, the slurries were foamed by vigorous mechanical mixing (2000 rpm) for 5 min after the addition of 4 wt.% Triton X-100 (polyoxyethylene octyl phenyl ether, Sigma-Aldrich, Gillingham, UK) and subsequently cast in polystyrene molds (50 mm diameter). The foams were

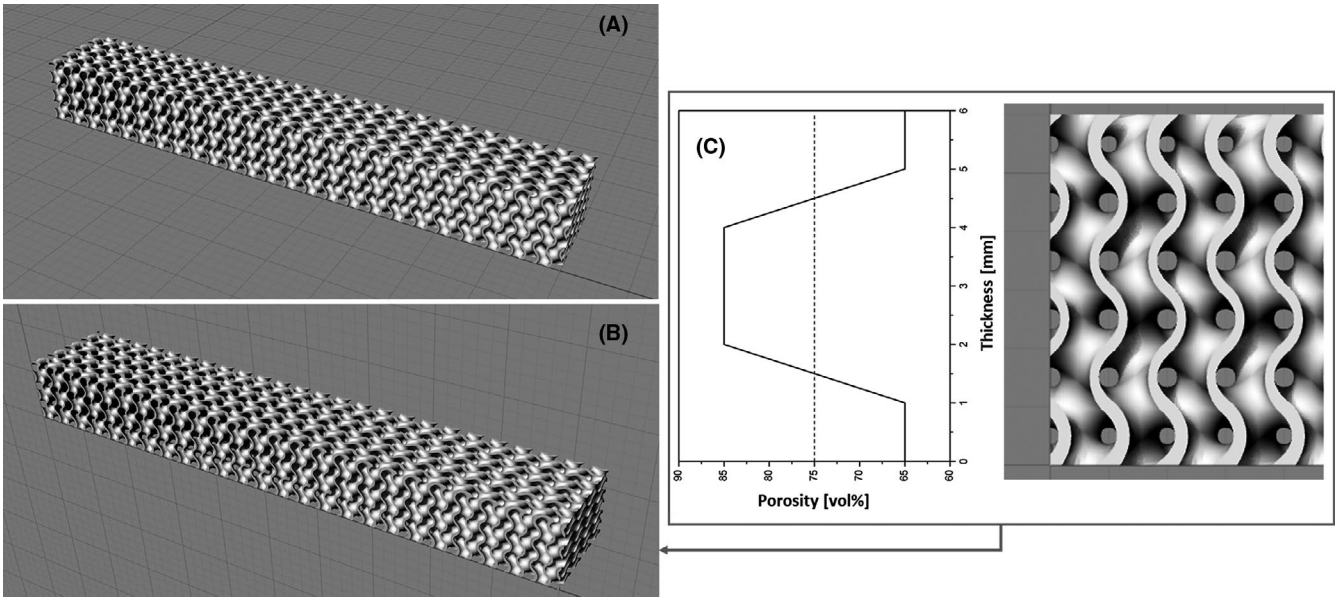

FIGURE 1 Details of reference three-dimensional models adopted for the fabrication of uniform (A) and graded (B) scaffolds, according to a specific porosity profile (C)

dried at 40°C for 24 h, demolded, and subjected to a preliminary heat treatment in air at 350°C (5°C/min heating rate) for 1 h for the burn-out of organics. Sintering (in air) was later performed with the same heating schedule adopted for scaffolds (1000°C for 1 h - 5°C/min heating rate -, followed by natural cooling).

2.4 | Characterization of cellular glass-ceramics

The evolution of samples was investigated on powdered samples, employing the Fourier transform IR spectroscopy (FTIR, FTIR model 2000, Perkin Elmer, Waltham, MA, USA) and X-ray diffraction (XRD; Bruker AXS D8 Advance, Bruker, Germany). The phase identification from diffraction patterns was performed using the Match!® program package (Crystal Impact GbR, Bonn, Germany), supported by data from the PDF-2 database (ICDD-International Centre for Diffraction Data, Newtown Square, PA).

The bulk density was computed from the weight-to-volume ratios on regular blocks (cut from bigger foamed samples or directly available from DLP), after careful determinations of weights and dimensions of the samples by analytical balance (precision of 0.0001 g) and a digital caliper, respectively. The apparent and true densities of various samples were measured by He gas pycnometry (Micromeritics AccuPyc 1330, Norcross, GA, USA), applied on samples both in bulk and powder forms. Morphological and microstructural characterizations were performed by optical stereomicroscopy (AxioCam ERc 5s Microscope Camera, Carl Zeiss Microscopy, Thornwood, New York, NY, USA) and scanning electron microscopy (FEI Quanta 200 ESEM, Eindhoven, The Netherlands).

Gyroid scaffolds, in the form of bars, as produced by the printing/sinter-crystallization process, with a cross section of about 4.6 mm × 3.5 mm, were subjected to 4-point bending tests (24 mm lower span, 8 mm upper span), at room temperature, employing a Galdabini Quasar 25 UTM material testing machine (Galdabini S.p.a., Cardano al Campo, Italy) operating with a cross-head speed of 1 mm/min. Each data point represents the average value of at least eight individual tests.

The compressive strength of foams and scaffolds was measured on small blocks cut from larger samples (blocks of about 10 mm × 10 mm × 8 mm for foams; blocks of about 4.6 mm × 3.5 mm × 6 mm for gyroid scaffolds, from the cutting of some printed/sinter-crystallized bars) employing the mechanical testing machine specified above, operating with a cross-head speed of 0.5 mm/min. Each data point represents the average value of at least 10 individual tests.

MG-63 human osteoblast-like cells (Sigma-Aldrich, Germany) were used to evaluate the cell behavior of selected samples (WDE gyroid scaffolds). This osteosarcoma cell line was cultured at 37°C in a humidified atmosphere of 95% air and 5% CO_2, in DMEM (Dulbecco's modified Eagle's medium, Gibco, Germany) containing 10 vol.% fetal bovine serum (FBS, Sigma-Aldrich, Germany) and 1 vol.% penicillin/streptomycin (Sigma-Aldrich, Germany). Cells were grown for 48 h to confluence in 75 cm^2 culture flasks (Sarstedt, Germany), washed with phosphate-buffered saline (PBS) before harvested using Trypsin/EDTA (Sigma, Germany), counted by a hemocytometer (Roth, Germany), and diluted to a final concentration of 100 000 cells/ml. The gyroid scaffolds were sterilized using dry heat (Nabertherm L3/11 B180, 160°C, 2 h). Each scaffold was incubated with 2 ml of cell suspension.

To analyze the adherent growth of cells on the WDE scaffolds, Vybrant™ DiI cell-labeling solution (Invitrogen, United States) was used to stain the cell membrane. After 7 days of incubation, the cell culture medium was removed, a staining solution (4 μl dye labeling solution to 1 ml of growth medium) was added and incubated for 45 min. Afterward, the staining solution was removed, the samples were washed with PBS (Gibco) and cells on the WDE samples were fixed by 10 vol.% formaldehyde in PBS.

Additionally, a DNA staining using DAPI was performed. For this, the PBS was removed, a DAPI staining solution (1 μl dye labeling solution to 1 ml PBS) was added and incubated for 5 min. The staining solution was removed and replaced with 2.5 ml PBS. Images were taken by fluorescence microscopy (Stemi 508, HXP 120 C, Zeiss, Germany).

3 | RESULTS AND DISCUSSION

3.1 | Advanced glass-ceramic scaffolds from additive manufacturing

Figure 2 illustrates the morphology of gyroid scaffolds in the after-printing state. In both geometries (homogeneous, Figure 2A, and graded, Figure 2B), the printing determined some coarsening of the structure defined by the models shown in Figure 1. This can be attributed to the loading effect of photocurable resin with a substantial glass content; in fact, the suspended particles are known to cause light scattering.[28] It should be noted that the adopted conditions of layer thickness and exposure time were the result of several trials and represent a compromise between resolution, integrity of samples, and practical feasibility. A closer match with the geometrical model could be ideally achieved with a shorter exposition time, to minimize the scattering. However, this approach complicated the hardening of the resin (thickness of

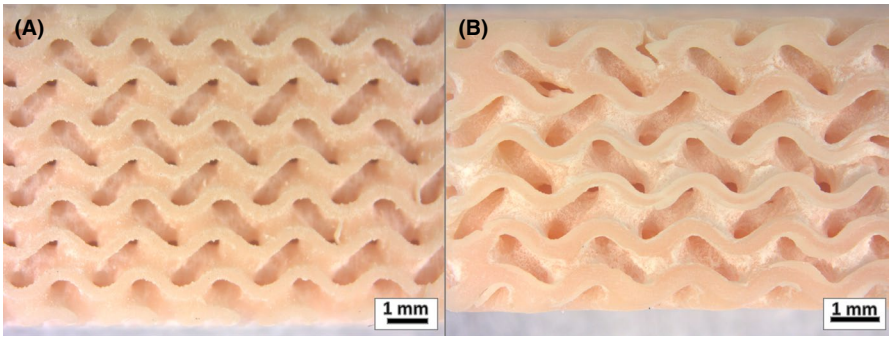

FIGURE 2 Details of printed resin-glass precursors of uniform (A) and graded (B) scaffolds

the cross-linked layer lower than layer thickness), leading to highly defective samples. The defectivity could be minimized by reducing the layer thickness, with much longer printing sessions, but this enhanced the risk of powder sedimentation.

As shown in Table 1, the total porosity of the fired products decreased, compared to the reference models, but it remained substantial (>45%), and completely open (Figure 3A). In fact, the firing resulted in a remarkable shrinkage (in the order of 42%), but no further coarsening of the cellular structures occurred, for both geometries, as shown by Figure 3B and C.

The preservation of the shape imparted by means of DLP printing was a fundamental objective and motivated the choice of a lower sintering temperature (1000°C) than in previous experiments.[18] In other words, avoiding the sealing of channels in new gyroid scaffolds (Figure 3D) had a higher priority compared to the complete densification of adjacent particles, which was desirable in the case of the struts of previous reticulated scaffolds, sintered at 1100°C.[18] Figure 3E showing the detail of a wall, testifies the limiting action on viscous flow densification operated by crystallization, with a multitude of crystals visible at the surface of not completely merged former glass particles (crystals, acting as rigid inclusions, increased the apparent viscosity).

Figure 4 illustrates that the starting material was X-ray amorphous except for a minor trace of quartz (PDF#85-0794) from unreacted raw materials. The pronounced crystallization of WDE glass, after sintering at 1000°C, could be noted from the strong diffraction maxima emerging from a nearly flat background. The two expected crystal phases, consisting of wollastonite ($CaSiO_3$, or $CaO{\cdot}SiO_2$, PDF#84-0665) and diopside ($CaMgSi_2O_6$, or $CaO{\cdot}MgO{\cdot}2SiO_2$, PDF#71-0655), are well defined, accompanied by åkermanite ($Ca_2MgSi_2O_7$, $2CaO{\cdot}MgO{\cdot}2SiO_2$, PDF#87-0046). This third phase does not represent an issue, since it is among the most promising Ca-Mg silicates for bone tissue engineering applications.[12,15]

Åkermanite likely formed due to the incomplete incorporation of SiO_2 in wollastonite and diopside, in analogy with studies on polymer-derived Ca-Mg silicate bioceramics ($CaSiO_3 + CaMgSi_2O_6 \leftrightarrow Ca_2MgSi_2O_7 + SiO_2$).[15] Previously investigated WDE-derived glass-ceramic scaffolds did not feature any traces of åkermanite, but it should be noted that the firing temperature was set at 1100°C,[18] thus favoring the ionic interdiffusion and the achievement of the phases expected from the thermodynamic equilibrium.

Compared to previous scaffolds (see Table 1), from the overlapping of cubic, diamond or Kelvin cells,[18] gyroid scaffolds exhibited enhanced mechanical properties - expressed by the far higher specific compressive strength

TABLE 1 Physical and mechanical properties of porous wollastonite-diopside glass-ceramics

Sample	Porosity (vol%)	Density, ρ (g/cm^3)	Compressive strength, σ_{cr} (MPa)	Specific compressive strength, σ_{cr}/ρ (MPa·cm^3/g)	Bending strength, σ_{bend} (MPa)	Bending strength index, $\sigma_{bend}^{2/3}/\rho$ (MPa$^{2/3}$·cm^3/g)
Diamond cell scaffold[18]	67	1.05 ± 0.03	15.2 ± 1.3	14.5		
Cubic cell scaffold[18]	77	0.72 ± 0.03	5.7 ± 1.5	7.9		
Uniform gyroid scaffold	48	1.67 ± 0.03	32.7 ± 8.7	19.6	24.6 ± 3.7	5.1
Graded gyroid scaffold	45	1.74 ± 0.02	32.2 ± 5.7	18.5	31.5 ± 2.8	5.7
Open-celled foam	81	0.61 ± 0.01	1.6 ± 0.4	2.6		
13-93 scaffold[30]	51	1.29	86 ± 4	66.2	15 ± 1	4.7
Cancellous bone		0.15-0.78[32]	0.6-11[32]	7.3[32]	10-20[30]	
Cortical bone[32]		1.8-2.1[32]	>100[32]	>51[32]	>50[30]	>7[32]

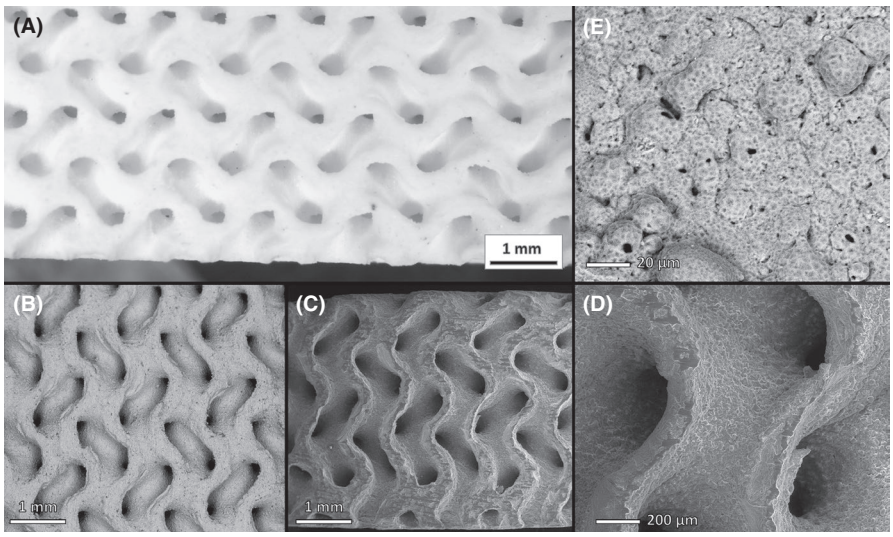

FIGURE 3 Microstructural details of fired scaffolds (counterclockwise): (A) top view (real colors, optical stereomicroscopy); (B) uniform scaffold; (C) graded scaffold; (D) walls; (E) sinter-crystallized particles

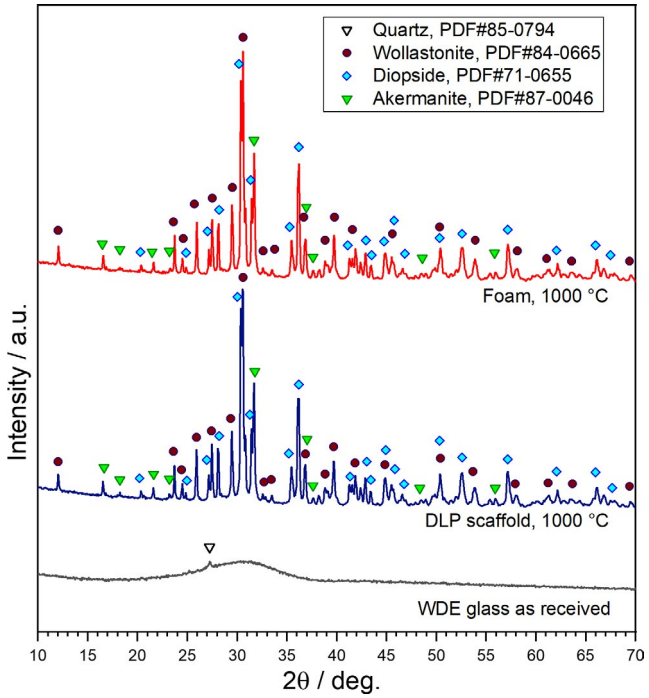

FIGURE 4 X-ray diffraction analysis of the starting glass and of the sinter-crystallized products (scaffold and foam)

(strength-to-density ratio, σ_{cr}/ρ) -, despite the microvoids (Figure 3E) left by some incomplete densification of walls. To our opinion, such an increase can be attributed to the specific topology, rather than to a different phase assemblage, with an enhancement of åkermanite. As mentioned previously, Ca-Mg silicates are well known to offer enhanced mechanical properties, compared to wollastonite,[12] but åkermanite was shown to be weaker than diopside.[29]

In terms of absolute values of compressive strength ($\sigma_{cr} > 30$ MPa), the obtained gyroid scaffolds fell well above the limits of cancellous bone.[30] However, they compared quite poorly with, for example, reticulated scaffolds (with a porosity of about 50%) from robocasting of 13-93 bioactive glass.[30] This fact, in our opinion, could be explained by the buckling of walls in the gyroid scaffolds. Buckling is reasonably limited in scaffolds from robocasting, in the case of well-overlapped filaments, oriented in 0-90° directions. The gyroid scaffolds counterbalanced the relative weakness in compression with remarkable bending strength values. In particular, gyroid scaffolds compared well with the previously mentioned 13-93 bioactive glass scaffolds already in the case of uniform porosity; graded scaffolds, as expected by locating more material far from the neutral axis of bending (enhancing the moment of inertia), led to a further improvement. The improvement is evident mainly from the index $\sigma_{bend}^{2/3}/\rho$ (an increase in ~12%), ruling the lightness of a bar under a specified applied bending moment (lightness increases with increasing index values).[31] The index value is still far lower than that of cortical bone ($\sigma_{bend}^{2/3}/\rho > 7$ MPa$^{2/3}$·cm^3/g)[32] but some improvements, in the future, are expected from refined structures, featuring a more substantial porosity gradient.

Preliminary cell tests, according to the protocol described above, were performed on WDE glass-ceramic scaffolds with uniform porosity. In agreement with the alkali-free condition, the immersion of samples in the cell culture medium did not result in any increase in pH. The initial pH was 7.94/8.08, whereas the value of 7.87/7.91 was achieved after 18 days. Fluorescence imaging revealed a homogeneous distribution of cells on the samples (see Figure 5A and B).

3.2 | Glass-ceramic foams from engineered activation of glass suspensions

Tissue engineering comprises also nonload-bearing components. Highly porous foams are typically appreciated for their

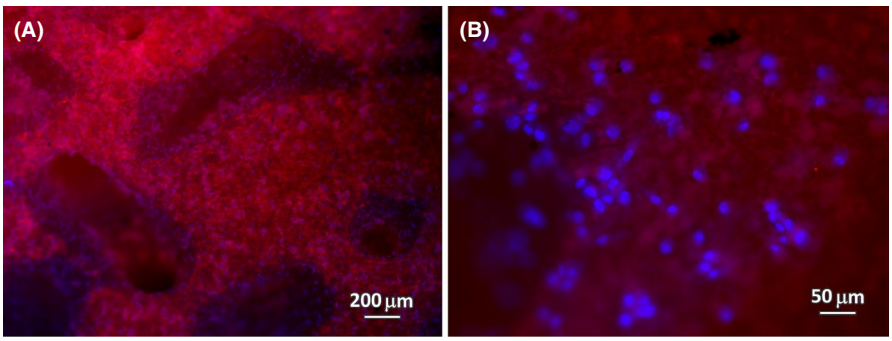

FIGURE 5 Surface of a Wollastonite-Diopside scaffold seeded with MG63 cells (A); blue fluorescence showing the DAPI-stained DNA (B)

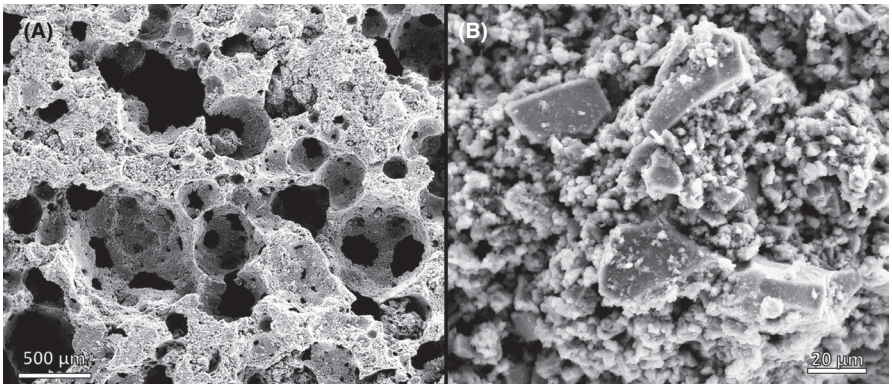

FIGURE 6 Microstructural details of a "green" foam from activation with TEAOH-containing solution: (A) overall cellular structure; (B) detail of a strut

ability to support the colonization of cells and the infiltration of body fluids.[33] Like in the case of DLP processing, supported by fugitive photocurable binders, highly porous glass-ceramics were studied with the main aim of minimizing the impact of the processing on the sinter-crystallization, with special attention paid to the preservation of the chemical composition. As mentioned previously, foams were manufactured by mechanical foaming ("frothing") of aqueous suspensions of fine glass powders, undergoing progressive gelation, followed by drying and viscous flow sintering. Any modification of the chemical composition was prevented by the replacement of alkaline activators, such as NaOH and KOH, with tetra-ethyl-ammonium hydroxide (TEAOH).

The only preliminary experience with BGMS10 bioactive glass[34] had referred to the gelation of glass suspensions operated by the interaction between glass powders and an aqueous solution of tetra-methyl-ammonium hydroxide ($[N(CH_3)_4]^+OH^-$,TMAH). The presence of four organic groups attached to a nitrogen atom, instead of hydrogen atoms, makes "quaternary substituted" compounds more basic than ammonium hydroxide ($[NH_4]^+OH^-$)[35] and a suitable alternative to NaOH, for example, in the activation of cellulose.[36] The replacement of TMAH with TEAOH was motivated by safety issues: the application of TMAH is, in fact, quite controversial, since its degradation leads to the evolution of hazardous tri-methyl-ammine.[37] TEAOH, on the contrary, is known for its applications in inorganic chemistry, for example, in the synthesis of zeolites.[38]

Figure 6 shows that the new activator had no negative impact on the effectiveness of gelation. Homogeneous "green" foams could be still obtained (Figure 6A), keeping the low molarity (1 M) of the activating aqueous solution and applying intensive mechanical stirring, with the help of Triton X-100 surfactant, to glass suspensions. WDE glass particles appeared to be surrounded by a gel phase (see Figure 6B).

The FTIR spectra in Figure 7A confirm the effectiveness of the attack of the basic activator. Well-defined bands appear only in the spectrum for activated glass, compared to the spectra for the material in as received and fired states. More precisely, the bands at 3000-3700 and 1650 cm^{-1}, attributable to O-H stretching and bending, express the hydration of WDE glass. The surfactant is distinguishable from the band at 2900 cm^{-1}. This band (attributed to CH_2 stretching) is actually shared with TEAOH, in turn justifying a number of characteristic signals in the spectrum for activated glass (as an example, CH_3 rocking and NC_4 stretching at 838 and 788 cm^{-1}, respectively).[39] We could not exclude, as a reason for the intense absorption peaks at 1400-1450 cm^{-1}, a contribution of C-O stretching vibrations in carbonates.[40]

Carbonation was effectively assessed by mineralogical analysis, shown in Figure 7B. Interestingly, it did not correspond to the formation of hydrated carbonate phases, as found with alkali-containing glasses and NaOH-based activation.[19] The particular basic attack, from Ca^{2+} ions released from WDE glass combined with CO_2 captured from the atmosphere, promoted the formation of anhydrous calcium carbonate phases. More precisely, most diffraction maxima match with $CaCO_3$ polymorphs (calcite, PDF#85-1108, and aragonite, PDF#41-1475). Only a few remaining diffraction

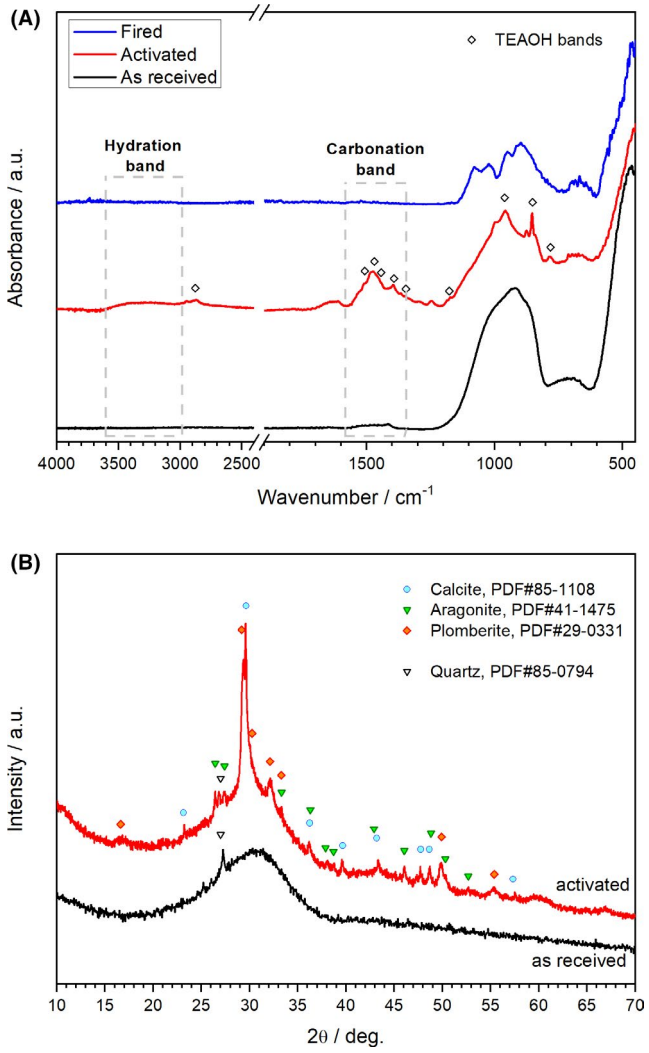

FIGURE 7 Assessment of the gelation of TEAOH-activated glass suspensions, by (A) infrared spectroscopy and (B) X-ray diffraction analysis

maxima are attributable to a calcium silicate hydrated (C-S-H) phase (namely plomberite, $Ca_5Si_6O_{16}(OH)_2{\cdot}8H_2O$, PDF#29-0331).The clear detection (by X-ray diffraction) of a phase normally found in cement hydration[41,42] is unprecedented, while the formation of calcium silicate hydrated compounds is in agreement with the basic attack of calcium silicate glasses.[19]

The hardening of WDE glass combined with TEAOH solution suggests applications even beyond the processing of bioactive glass-ceramics, such as CO_2 capture and replacement of conventional types of cement in constructions (in analogy with wollastonite-based cements),[43] which will constitute the focus of future experiments. In any case, the particular phases developed upon activation did not compromise the development of homogeneous glass-ceramic foams after firing at 1000°C (Figure 8A). As shown in Figure 4, fired foams had a good match, in terms of developed phases (wollastonite, diopside, and åkermanite), with gyroid scaffolds.

Foams were far more porous than gyroid scaffolds. Besides macro-pores already present in the hardened suspensions ("green" foams, as shown in Figure 6A), smaller pores could be seen in the struts (see Figure 8B). The WDE glass went through a "reactive" sinter-crystallization, that is, the particles underwent sintering with concurrent thermal decomposition of the gel phase. The gas generation (release of CO_2 and water vapor) led to a sort of "secondary" foaming, as observed for gels from NaOH activation.[19] The microporosity is reputed as being favorable for cell attachment and infiltration of body fluids. As reported in Table 1, both compressive strength and strength-to-density ratio were far lower than those available from scaffolds, even in the most porous variants (diamond-celled scaffolds) developed previously.[18] Nevertheless, the strength and porosity data were comparable to those achieved from polymer-derived wollastonite-diopside foams.[15]

4 | CONCLUSIONS

An alkali-free glass, obtained from a melt corresponding to the eutectic between wollastonite ($CaSiO_3$) and diopside ($CaMgSi_2O_6$), was easily converted into a silicate-based glass-ceramic, by sinter-crystallization of fine powders. The adopted sintering temperature, 1000°C, lower than that previously used, yielded åkermanite ($Ca_2MgSi_2O_7$) as

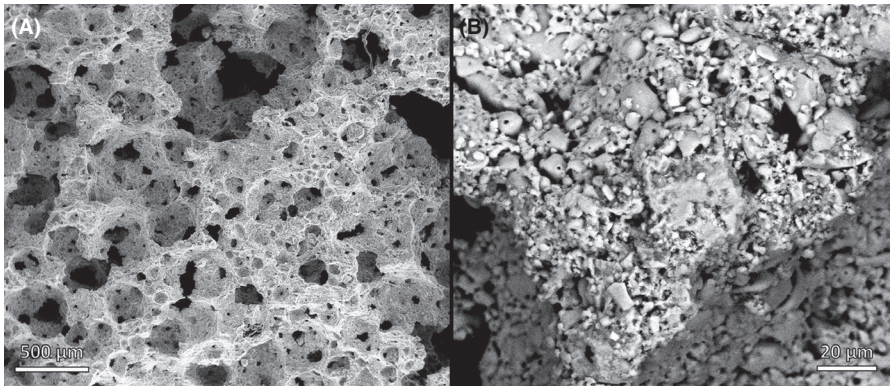

FIGURE 8 Microstructural details of a fired WDE foam: (A) overall cellular structure; (B) detail of a strut

an additional phase, besides wollastonite and diopside. The preliminary cell test confirmed the cytocompatibility of the material in contact with osteoblast-like bone cells, consistently with the inclusion of all developed phases, among the most promising silicate biomaterials. High strength porous components, especially when loaded in bending configuration, may be achieved by digital light processing of powders suspended in a sacrificial, commercial photocurable binder, adopting a gyroid scaffold geometry; the specific topology could be tuned to further increase the bending strength, according to graded structures. As an alternative, highly porous foams were produced by a facile gel casting method, by the hardening of glass powders suspended in aqueous solution, activated with tetra-ethyl-ammonium hydroxide. The adoption of this particular base led to the development of unprecedented hardening compounds, such as a well-crystallized calcium silicate hydrate and anhydrous $CaCO_3$ polymorphs, implying possible application of the adopted glass even beyond biomaterials. The new gel casting process kept the simplicity of activation with inorganic bases, such as NaOH, but it did not affect the chemical composition of the glass, as in the additive manufacturing approach.

ACKNOWLEDGEMENTS

This paper is a part of the dissemination activities of project FunGlass (Centre for Functional and Surface Functionalized Glass). This project has received funding from the European Union's Horizon 2020 research and innovation programme under grant agreement no 739566. The authors thank Mr Andrea Mazzer, Mr Matteo Sottoriva and Mr Riccardo Sponchiado (University of Padova) for experimental assistance. Helpful discussions with Dr. Rainer Detsch and Ms Alina Gruenewald (Institute of Biomaterials, Erlangen) are highly appreciated.

ORCID

Hamada Elsayed https://orcid.org/0000-0002-9818-4498
Patricia Rabelo Monich https://orcid.org/0000-0003-0436-8091
Gianpaolo Savio https://orcid.org/0000-0001-5858-1483
Aldo R. Boccaccini https://orcid.org/0000-0002-7377-2955
Dusan Galusek https://orcid.org/0000-0001-5995-8780
Enrico Bernardo https://orcid.org/0000-0003-4934-4405

REFERENCES

1. Hench LL, Pantano CG, Buscemi PJ, Greenspan DC. Analysis of bioglass fixation of hip prostheses. J Biomed Mater Res. 1977;11:267–82.
2. Hench LL. Opening paper 2015- Some comments on Bioglass: Four Eras of Discovery and Development. Biomed Glasses. 2015;1:1–11.
3. El-Rashidy AA, Roether JA, Harhaus L, Kneser U, Boccaccini AR. Regenerating bone with bioactive glass scaffolds: a review of in vivo studies in bone defect models. Acta Biomater. 2017;62:1–28.
4. Peitl O, Dutra Zanotto E, Hench LL. Highly bioactive P_2O_5–Na_2O–CaO–SiO_2 glass-ceramics. J Non Cryst Solids. 2001;292:115–26.
5. Kido HW, Oliveira P, Parizotto NA, Crovace MC, Zanotto ED, Peitl-Filho O, et al. Histopathological, cytotoxicity and genotoxicity evaluation of Biosilicate® glass-ceramic scaffolds. J Biomed Mater Res Part A. 2013;101A:667–73.
6. Ciraldo FE, Boccardi E, Melli V, Westhauser F, Boccaccini AR. Tackling bioactive glass excessive in vitro bioreactivity: preconditioning approaches for cell culture tests. Acta Biomater. 2018;75:3–10.
7. Goel A, Kapoor S, Rajagopal RR, Pascual MJ, Kim H-W, Ferreira JMF. Alkali-free bioactive glasses for bone tissue engineering: a preliminary investigation. Acta Biomater. 2012;8:361–72.
8. Kansal I, Tulyaganov DU, Pascual MJ, Gremillard L, Malchere A, Ferreira JMF. Sintering behaviour of diopside ($CaO•MgO•2SiO_2$)–fluorapatite ($9CaO•3P_2O_5•CaF_2$) bioactive glass. J Non Cryst Solids. 2013;380:17–24.
9. Brito AF, Antunes B, dos Santos F, Fernandes HR, Ferreira JMF. Osteogenic capacity of alkali-free bioactive glasses. In vitro studies. J Biomed Mater Res Part B Appl Biomater. 2017;105:2360–5.
10. Kapoor S, Goel A, Correia AF, Pascual MJ, Lee HY, Kim HW, et al. Influence of ZnO/MgO substitution on sintering, crystallisation, and bio-activity of alkali-free glass-ceramics. Mater Sci Eng C. 2015;53:252–61.
11. Kokubo T, Shigematsu M, Nagashima Y, Tashiro M, Nakamura T, Yamamuro T, et al. Apatite- and wollastonite-containg glass-ceramics for prosthetic application. Bull Inst Chem Res Kyoto Univ. 1982;60:260–8.
12. Wu C, Chang J. Degradation, bioactivity, and cytocompatibility of diopside, akermanite, and bredigite ceramics. J Biomed Mater Res Part B Appl Biomater. 2007;83B:153–60.
13. Sunouchi K, Tsuru K, Maruta M, Kawachi G, Matsuya S, Terada Y, et al. Fabrication of solid and hollow carbonate apatite microspheres as bone substitutes using calcite microspheres as a precursor. Dent Mater J. 2012;31:549–57.
14. No Y, Li J, Zreiqat H. Doped calcium silicate ceramics: a new class of candidates for synthetic bone substitutes. Materials. 2017;10:153.
15. Fiocco L, Li S, Stevens MM, Bernardo E, Jones JR. Biocompatibility and bioactivity of porous polymer-derived Ca-Mg silicate ceramics. Acta Biomater. 2017;50:56–67.
16. Sainz MA, Pena P, Serena S, Caballero A. Influence of design on bioactivity of novel $CaSiO_3$–$CaMg(SiO_3)_2$ bioceramics: in vitro simulated body fluid test and thermodynamic simulation. Acta Biomater. 2010;6:2797–807.
17. Ros-Tárraga P, Mazón P, Sainz MA, Meseguer-Olmo L, De Aza PN. Surface modifications of a diopside–wollastonite eutectic ceramic after acellular and cellular in vitro tests. Surf Coatings Technol. 2019;378:124965.
18. Elsayed H, Schmidt J, Bernardo E, Colombo P. Comparative analysis of wollastonite-diopside glass-ceramic structures fabricated via stereo-lithography. Adv Eng Mater. 2019;21:1801160.
19. Elsayed H, Rincón Romero A, Ferroni L, Gardin C, Zavan B, Bernardo E. Bioactive glass-ceramic scaffolds from novel 'inorganic gel casting' and sinter-crystallization. Materials. 2017;10:171.

20. Baino F, Ferraris M, Bretcanu O, Verné E, Vitale-Brovarone C. Optimization of composition, structure and mechanical strength of bioactive 3-D glass-ceramic scaffolds for bone substitution. J Biomater Appl. 2013;27:872–90.
21. Wu ZY, Hill RG, Yue S, Nightingale D, Lee PD, Jones JR. Melt-derived bioactive glass scaffolds produced by a gel-cast foaming technique. Acta Biomater. 2011;7:1807–16.
22. Yan C, Hao L, Hussein A, Raymont D. Evaluations of cellular lattice structures manufactured using selective laser melting. Int J Mach Tools Manuf. 2012;62:32–8.
23. Yánez A, Herrera A, Martel O, Monopoli D, Afonso H. Compressive behaviour of gyroid lattice structures for human cancellous bone implant applications. Mater Sci Eng C. 2016;68:445–8.
24. Baino F, Fiume E, Barberi J, Kargozar S, Marchi J, Massera J, et al. Processing methods for making porous bioactive glass-based scaffolds—a state-of-the-art review. Int J Appl Ceram Tech. 2019;16:1762–96.
25. Sepulveda P, Binner JG. Processing of cellular ceramics by foaming and in situ polymerisation of organic monomers. J Eur Ceram Soc. 1999;19:2059–66.
26. Gonzenbach UT, Studart AR, Steinlin D, Tervoort E, Gauckler LJ. Processing of particle-stabilized wet foams into porous ceramics. J Am Ceram Soc. 2007;90:3407–14.
27. Savio G, Meneghello R, Concheri G. Design of variable thickness triply periodic surfaces for additive manufacturing. Prog Addit Manuf. 2019;4:281–90.
28. Gentry SP, Halloran J. Light scattering in absorbing ceramic suspensions: effect on the width and depth of photopolymerized features. J Eur Ceram Soc. 2014;35:1895–904.
29. Najafinezhad A, Abdellahi M, Ghayour H, Soheily A, Chami A, Khandan A. A comparative study on the synthesis mechanism, bioactivity and mechanical properties of three silicate bioceramics. Mat Sci Eng C. 2017;72:259–67.
30. Eqtesadi S, Motealleh A, Pajares A, Guiberteau F, Miranda P. Improving mechanical properties of 13–93 bioactive glass robocast scaffold by poly (lactic acid) and poly (ε-caprolactone) melt infiltration. J Non Cryst Solids. 2016;432:111–9.
31. Ashby MF. Materials selection in mechanical design (3rd edition). Oxford: Butterworth Heinemann; 2005.
32. CES EduPack 2020 materials education software.
33. Chen QZ, Thompson ID, Boccaccini AR. 45S5 Bioglass®-derived glass–ceramic scaffolds for bone tissue engineering. Biomaterials. 2006;27:2414–25.
34. Elsayed H, Rincon Romero A, Bellucci D, Cannillo V, Bernardo E. Advanced open-celled structures from low-temperature sintering of a crystallization-resistant bioactive glass. Materials. 2019;12:3653.
35. Lobodin VV, Juyal P, McKenna AM, Rodgers RP, Marshall AG. Tetramethylammonium hydroxide as a reagent for complex mixture analysis by negative ion electrospray ionization mass spectrometry. Anal Chem. 2013;85:7803–8.
36. Tanczos I, Borsa J, Sajó I, László K, Juhász ZA, Tóth T. Effect of tetramethylammonium hydroxide on cotton cellulose compared to sodium hydroxide. Macromol Chem Phys. 2000;201:2550–6.
37. Lei CN, Whang LM, Lin HL. Biological treatment of thin-film transistor liquid crystal display (TFT-LCD) wastewater. Water Sci Technol. 2008;58:1001–6.
38. He D, Yuan D, Song Z, Tong Y, Wu Y, Xu S, et al. Hydrothermal synthesis of high silica zeolite Y using tetraethylammonium hydroxide as structure-directing agents. Chem Commun. 2016;86:12765–8.
39. Gao H, Li J, Lian K. Alkaline quaternary ammonium hydroxides and their polymer electrolytes for electrochemical capacitors. RSC Adv. 2014;4:21332–9.
40. García Lodeiro I, Fernández-Jimenez A, Palomo A, Macphee DE. Effect on fresh C-S-H gels of the simultaneous addition of alkali and aluminium. Cem Concr Res. 2010;40:27–32.
41. Bonaccorsi E, Merlino S, Kampf AR. The crystal structure of tobermorite 14 Å (Plombierite), a C-S-H phase. J Am Ceram Soc. 2005;88:505–12.
42. Kalinichev AG, Wang J, Kirkpatrick RJ. Molecular dynamics modeling of the structure, dynamics and energetics of mineral–water interfaces: application to cement materials. Cem Concr Res. 2007;37:337–47.
43. Svensson K, Neumann A, Menezes FF, Lempp C, Pöllmann H. The conversion of wollastonite to $CaCO_3$ considering its use for CCS application as cementitious material. Appl Sci. 2018;8:304.

How to cite this article: Elsayed H, Rabelo Monich P, Savio G, et al. Alkali-free processing of advanced open-celled sinter-crystallized glass-ceramics. *Int J Appl Glass Sci*. 2021;12:531–540.

https://doi.org/10.1111/ijag.16106